Physics Based Control Oriented Model for HCCI Combustion Timing

Mahdi Shahbakhti*and Charles Robert Koch†
Department of Mechanical Engineering, University of Alberta
Edmonton, Alberta, Canada

Abstract

Incorporating Homogeneous Charge Compression Ignition (HCCI) into combustion engines for better fuel economy and lower emission requires understanding the dynamics influencing the combustion timing in HCCI engines. A control oriented model to dynamically predict cycle-to-cycle combustion timing of an HCCI engine is developed. The model is designed to work without parameters that are difficult to measure and have low computation time with sufficient accuracy for control applications. The model is a full cycle model and consists of a residual gas model, a modified knock integral model, fuel burn rate model, and thermodynamic models. In addition, semi-empirical correlations are used to predict the gas exchange process generated work and completeness of combustion. The developed model incorporates the thermal coupling dynamics caused by the residual gases from one cycle to the next cycle. The amount of residual gas is calculated using an iterative process based on the amount of mass retained inside the cylinder when exhaust valves close. The model is parameterized by over 5700 simulations from a detailed thermo-kinetic model and experimental data obtained

*e-mail:M.Shahbakhti@ualberta.ca
†Corresponding author: 4-9, Mechanical Engineering Building, University of Alberta, Edmonton AB T6G 2G8, Canada; phone: 780-492-8821; fax: 780-492-2200; e-mail:bob.koch@ualberta.ca

from a single-cylinder engine. Cross validation of the model with both steady-state and transient HCCI experiments for four different Primary Reference Fuel (PRF) blends is detailed. With seven model inputs, the combustion timing of over 150 different HCCI points is predicted to within an average error of less than 1.5 degrees of crank angle. A narrow window of combustion timing is found to provide stable and efficient HCCI operation.

Nomenclature

Symbols

A	Area [m^2].
AFR	Air Fuel ratio [-].
$CA50$	Crank angle for 50% burnt fuel [CAD aTDC].
C_D	Discharge coefficient [-].
C_v	Constant-volume specific heat capacity [$\frac{kJ}{kg.K}$].
C_p	Constant-pressure specific heat capacity [$\frac{kJ}{kg.K}$].
C_r	Compression ratio [-].
CoC	Newtonian reference frame.
CoC	Completeness of combustion [-].
d_v	Exhaust valve diameter [m].
EGR	Fraction of exhaust gas recirculated [-].
f_c	Cutoff frequency [$\frac{1}{CAD}$].
h	Enthalpy [$\frac{kJ}{kg}$].

h_c Convective heat transfer coefficient $[\frac{W}{m^2.K}]$.

k Ratio of specific heat capacities [-].

L Instantaneous cylinder height [m].

L_v Exhaust valve axial lift [m].

LHV Lower heating value of fuel $[\frac{kJ}{kg}]$.

m Mass [kg], but [g] in Eq. (34).

N Engine speed [rpm].

Φ Equivalence ratio [-].

OF Overlap factor [-].

PW Pulse width [ms].

P Pressure [kPa].

Q Heat [kJ].

R Gas constant $[\frac{kJ}{kg.K}]$, but $[\frac{J}{kg.K}]$ in Eq. (31).

ρ Density $[\frac{kg}{m^3}]$.

S_p Piston speed $[\frac{m}{s}]$.

t Time [s].

T Temperature [K], but [C] in Eq. (1) and (2).

θ Crank angle [CAD].

U Internal energy [kJ].

V Volume $[m^3]$.

W Work [kJ].

X_r Residual gas mass fraction [-].

X_d Mixture dilution fraction [-].

y	Mass fraction [-].

Abbreviations

aBDC	after Bottom Dead Center.
aTDC	after Top Dead Center.
AFR	Air Fuel Ratio.
CAD	Crank Angle Degree.
CFD	Computational Fluid Dynamics.
CI	Compression Ignition.
CO	Carbon Monoxide.
CO_2	Carbon Dioxide.
CV	Control Volume.
ECU	Engine Control Unit.
EGR	Exhaust Gas Recirculation.
EOC	End of Combustion.
EVC	Exhaust Valve Closing.
EVO	Exhaust Valve Opening.
HC	Hydrocarbons.
HCCI	Homogeneous Charge Compression Ignition.
H_2O	Water Vapor.
IMEP	Indicated Mean Effective Pressure.
IVC	Intake Valve Closing.

IVO	Intake Valve Opening.
KIM	Knock Integral Model.
MKIM	Modified Knock Integral Model.
NASA	National Aeronautics & Space Administration.
N_2	Nitrogen Gas.
NOx	Oxides of Nitrogen.
O_2	Oxygen Gas.
ON	Octane Number.
PM	Particulate Matter.
PRF	Primary Reference Fuel.
P	Products.
R	Reactants.
SI	Spark Ignition.
SOC	Start of Combustion.
TDC	Top Dead Center.
TKM	Thermo-Kinetic Model.
UEGO	Universal Exhaust Gas Oxygen (sensor).

Subscripts

a	air.
b	burned.
c	compression.

ce	(flow) from cylinder to exhaust.
ch	charge (air+fuel+EGR).
d	duration.
dis	displacement.
e	expansion.
ec	(flow) from exhaust to cylinder.
exh	exhaust.
egr	exhaust gas recirculated.
eoc	end of combustion.
evc	exhaust valve closing.
evo	exhaust valve opening.
f	fuel.
g	cylinder gas.
i	cycle/specie number.
iso	isooctane.
inj	injected.
ivc	intake valve closing.
ivo	intake valve opening.
m	(intake) manifold .
mod	modified.
r	residual gas.
R	Reference.
o	upstream of exhaust valves.

r	residual gas.
s	(in-cylinder) surface.
soc	start of combustion.
t	total gas.
T	downstream of exhaust valves.
v	(exhaust) valve.
w	cylinder walls.

1 Introduction

Homogeneous Charge Compression Ignition (HCCI) is an alternative principle for combustion engines that holds promises of low fuel consumption and low exhaust emissions in terms of Nitric Oxides (NOx) and Particulate Matter (PM) in the potential operating range [1, 2]. HCCI combustion relies on the auto-ignition of a compressed air-fuel mixture at local hot spots distributed through the mixture [3]. The mixture is homogeneous and the combustion temperature is low which minimizes the PM and NOx emissions. The mixture is compression ignited using high compression ratios and has low throttling losses and shorter combustion duration which leads to high efficiency. Lower cyclic variation of combustion is another benefit of HCCI [4]. This is important as high cyclic variations in engines can limit the operating range [5]. The HCCI benefits are accompanied by several major drawbacks including limited operating range and high unburned Hydrocarbon (uHC) and Carbon Monoxide (CO) emissions [6]. In order to obtain HCCI benefits and overcome the drawbacks, the most significant challenge is the control of HCCI combustion timing [7, 8]. Combustion timing

influences the magnitude of cyclic variations and the limits for which an HCCI engine can operate smoothly [9, 10]. One way to extend the operating range is use of a HCCI/Spark Ignition (SI) or HCCI/Compression Ignition (CI) dual-mode operation [11, 12]. This requires a precise control of HCCI combustion timing due to the sensitivity of HCCI combustion timing to the residual gas temperature and the different exhaust temperatures in each of these modes [13]. Combustion timing also influences the engine emissions, with regard to combustion and post-combustion temperatures [8, 14] and the residual gas composition and temperature for the next cycle [15]. Controlling HCCI combustion timing is essential for good engine performance but it is a challenging control problem because premixed HCCI lacks a direct mean to initiate the combustion. The combustion timing is governed by the mixture conditions characterized by not only the intake charge conditions but also by the temperature and composition state from the previous cycles.

Simulation models serve as a tool for understanding the dynamics of engine charge variations on combustion timing and are essential for subsequent control. Since chemical kinetics govern the HCCI auto-ignition, an understanding of them is usually contained in the simulation model. Depending on the purpose, there is a wide range of HCCI combustion models in the literature that are different in the level of complexity and the level of details in the kinetic mechanism. Detailed Thermo-Kinetic Models (TKM) include 1) Coupled CFD-kinetic TKMs [16]; 2) Sequential CFD based multi-zone TKMs [17]; 3) Multi-zone TKMs [18]; and 4) Zero dimensional TKMs [19]. While coupled CFD-kinetic TKMs with extensive computation are good for accurate prediction of engine's emissions, single zone TKMs are useful tools for predicting overall performance [20] with lower computational requirements. Extensive computation time in the TKMs makes them impractical for direct control applications on

engines except for single zone TKMs that apply a reduced order kinetic mechanism [21]. However, detailed complex TKMs can be used to develop control oriented models [22]. For control design purposes low-order models with short computation time are needed. Figure 1 shows the main categories of the control oriented models used to predict combustion timing for HCCI engines. Control oriented models are grouped into two main categories of models. The first category is intended to predict HCCI combustion timing for steady-state operation. The output of these models provides mean-value combustion timing. These models lack cyclic transition dynamics from one cycle to the next cycle. However, they can be augmented with other models to consider cycle-to-cycle interactions. This raises these models to the second category of the models that are appropriate not only for steady-state operation but also for transient operation. The second category of the models can be used for cycle-to-cycle control of HCCI combustion to manage the transition between different load-speed regions and also mode transition between HCCI operation and SI or CI operation.

The first category of the models include 1) simple look-up table approach [23] or temperature threshold method [24]; 2) Shell model [25, 26]; 3) Arrhenius-type rate threshold models [24, 27, 28, 29]; 4) knock integral models [30, 31, 32, 33]; 5) Modified Knock Integral Models, MKIM [22, 34, 35]. These models mainly differ in the level of accuracy and the required input data. For instance, the temperature threshold method is simple and doesn't need expensive inputs but it is not accurate at different operating conditions, while original Arrhenius-type models are more accurate but they need instantaneous fuel and oxygen concentrations and in-cylinder gas temperature that are difficult to measure[1]. The category II (transient) mod-

[1]In [36], the need for instantaneous parameters is removed by modifying the Arrhenius rate threshold model.

els can be organized into three main groups. The first group are the physic-based models [13, 28, 37, 38, 39] that are developed based on the category I (steady-state) models. These models are mainly thermodynamic models that include exhaust/residual thermal feedback dynamics from one cycle to the next cycle. The second group are the estimated discrete-time state-space models [40, 41] obtained from applying system identification methods for different load ranges. The third group are chaotic models [42, 43] that are based on the recognition that low order models can represent chaotic response.

This study is based on developing a new dynamic physics based control oriented model to predict cycle-to-cycle combustion phasing for an HCCI engine. The goal is to have a model that: can predict HCCI combustion timing cycle-to-cycle; has a good compromise between accuracy and computation time; and doesn't require inputs that are difficult to measure real-time on an engine. CA50, the crank angle where 50% of the mass fraction of fuel is burnt, is chosen because it is a good and robust indicator of HCCI combustion [44] and CA50 can be reliably used for feedback control of HCCI combustion [45]. A mean-value model of HCCI combustion from our previous works [46, 47] is extended to a full-cycle simulation model that considers the dynamics of cycle-to-cycle thermal coupling. The resulting model is validated by both steady-state and transient experimental data. The results demonstrate that the model can predict combustion phasing (CA50) for a range of experimental steady state and transient conditions.

In this paper, section two describes the structure of the model and the methodology to parameterize the model. Next, the experimental setup to collect steady-state and transient data is explained. Then, validation results of the model are discussed in section four and

finally conclusions are reached.

2 Model Description

An HCCI operating cycle is broken down into a sequence of valve events that include: intake stroke, compression stroke, combustion, expansion stroke, and exhaust stroke. The complete cycle simulation of an HCCI engine is done by building and linking the models for each part. The whole combustion chamber is assumed as a single zone with a uniformly distributed mixture. The models used to simulate the process for each part are explained in this section.

2.1 Intake Stroke (IVO → IVC)

2.1.1 IVC temperature & pressure correlation

In a premixed HCCI engine only during the intake stroke can the combustion timing be directly influenced. Although the intake process commences by the intake valves opening, it is the mixture condition at Intake Valve Closing (IVC) moment that predominantly determines the HCCI combustion timing [46]. It is difficult and expensive to measure the mixture temperature and pressure at IVC moment, but the intake temperature and intake pressure are usually measured in the intake manifold in the production engines. Two simple semi-empirical correlations are used for the intake process to estimate the pressure and temperature of the mixture at IVC from the measured values of the intake manifold. These correlations are parameterized using the experimental and simulation data.

An IVC pressure correlation from a previous study [46] is parameterized using the steady-

state experimental data collected for this study. Conditions of the experimental data are detailed later in the section 3. Half of the steady-state experimental data is used to parameterize the correlation and the other half is used to validate the correlation. The resulting correlation for the in-cylinder pressure at IVC (P_{ivc}) is:

$$P_{ivc} = \frac{N^{0.027}\ \Phi^{0.046}}{T_m^{0.005}} P_m \tag{1}$$

where, N is the engine speed in rpm, and P_m and T_m are the gas pressure and temperature in the intake manifold in kiloPascals (kPa) and in Celsius (°C) respectively and Φ is the equivalence ratio. The correlation suggests that P_{ivc} increases when intake pressure or engine speed increases, but P_{ivc} decreases when T_m increases or intake charge becomes leaner (Φ decreases). This is attributed to the influence of these parameters on the charge mass that can be inducted into the cylinder before IVC. An error analysis on correlation (1) results in an average error of 2.1 kPa and a standard deviation error of 1.8 kPa when applying the correlation on the other half of the steady-state experimental data that was not used to parameterize the correlation.

HCCI combustion is the most sensitive to T_{ivc} variations [36, 9] but it is very difficult and expensive to experimentally measure it. Here, T_{ivc} is estimated by using simulation results of a detailed thermo-kinetic model. Simulated T_{ivc} values that match experimental combustion timing are chosen as the correct T_{ivc} [46]. A detailed HCCI Thermo-Kinetic Model [48] for an arbitrary blends of PRF mixture of n-Heptane and Isooctane is run to obtain the values of T_{ivc}. This TKM uses a chemical kinetic mechanism consisting of 58 species and 102 reactions and can predict the Start of Combustion (SOC) for the Ricardo engine with an

average error of less than 0.8 CAD over a range of equivalence ratios, intake temperatures, intake pressures, EGR rates, PRF blends, and engine speeds [60]. Here, the TKM is run for the same experimental points used to parameterize correlation (1). The obtained values for T_{ivc} are used to parameterize the following correlation [49] to predict the temperature of air-fuel mixture at IVC. Table 1 indicates the values of the estimated parameters.

$$T_{ivc} = \left(A\ T_m^2 + B\ T_m + C\right) \frac{\Phi^D\ .\ N^E}{(1+EGR)^F} \tag{2}$$

where A, B, C, D, E and F are the parameters of the correlation that are determined and EGR is the rate of Exhaust Gas Recirculation. The correlation is found to be octane number dependent. It should be noted that T_m is measured after the inclusion of EGR gases, so the charge heating effect of EGR is already included in the measured T_m (engine experimental setup in section 3).

Table 1: Values of parameters for the T_{ivc} correlation

Parameter	**PRF0**[2]	**PRF10**	**PRF20**	**PRF40**
A	-0.0073	-0.0017	-0.0017	-0.0007
B	1.4829	0.4073	0.5533	0.3470
C	110.3672	101.2723	113.4466	112.3506
D	-0.1488	-0.0431	-0.1164	-0.0051
E	-0.0850	-0.0162	-0.0426	-0.0175
F	0.0092	0.0024	0.0002	0.0012

An analysis of equation (2) indicates that T_{ivc} is most sensitive to the intake manifold temperature and engine speed compared to EGR and Φ, with EGR having the least influence on T_{ivc}. As mentioned above the heating effect of EGR is already included in the measured

[2]PRF number is defined as the volume percentage of Isooctane in fuel mixture of n-Heptane and Isooctane.

T_m and the EGR term in equation (2) includes other EGR effects (e.g. dilution/chemical) on T_{ivc}. The quadratic term for the influence of T_m on T_{ivc} results in a change in the direction of heat transfer between the in-cylinder gases and the cylinder wall when the in-cylinder gas temperature becomes higher than that of the cylinder wall [49]. This observation has been also confirmed with our HCCI thermo-kinetic simulation model [48]. For a constant T_m, Φ and cylinder wall temperature (T_w), correlation (2) suggests that T_{ivc} decreases with increasing engine speed and increasing EGR rate. This can be explained by less available heating time (from the cylinder wall to the charge) at higher engine speeds. Also when EGR rate increases the total heat capacity of the charge increases[3][50]. This higher heat capacity reduces the amount of possible increase in the charge temperature during the heat transfer process between the charge and the cylinder wall with a constant T_w. Correlation (2) is cross-validated using the same data points used to test correlation (1) with the half of the data that is not used to parameterize the correlation. The results show an average error of 2.2 °C and standard deviation error of 1.9 °C.

2.1.2 Residual gas model (initial value)

Residual gas from the previous cycles influence the mixture conditions at IVC in terms of the temperature, composition and the dilution level. The residual gas causes inherent thermal cycle-to-cycle dynamics. These dynamics are important when designing HCCI transition particularly when the amount of internal EGR is altered by variable valve timing [38]. The thermal cyclic interaction is even more important for HCCI/SI or HCCI/CI modal transitions

[3]This heat capacity effect also delays HCCI auto-ignition timing and prolongs the combustion duration when EGR is increased. [50]

due to different residual gas temperatures when switching from one mode to the other [13].

In this study, the composition of the residual gas is considered to be a combination of combustion products for a complete, lean combustion that consists of H_2O, CO_2, N_2 and O_2 gases. Residual gas fraction (X_r) is defined as:

$$X_r = \frac{m_r}{m_t} \qquad ; \qquad m_t = m_a + m_{egr} + m_f + m_r \tag{3}$$

where, m presents the mass and indexes of a, egr, f, r and t respectively stand for air, EGR, fuel, residual gas and total when the intake valves are closed. Two major sources of residual gas are 1) the trapped exhaust gas before Intake Valve Opening (IVO) and 2) the back-flow of the exhaust gas into the cylinder during the valve overlap period. In HCCI engines, X_r is mainly dependant on valve timing, engine speed, fuel amount, intake manifold pressure and exhaust manifold pressure [51]. A model [52] is used to get an starting value for the value of X_r:

$$X_r = \overbrace{\sqrt{\frac{1}{C}\,\frac{\pi\sqrt{2}}{360}\,\frac{r_c-1}{r_c}\,\frac{OF}{N}\sqrt{\frac{R\,T_m|P_{exh}-P_m|}{P_{exh}}}\left(\frac{P_{exh}}{P_m}\right)^{\frac{k+1}{2k}}}}^{\alpha} + \overbrace{\frac{1}{C}\,\frac{r_c-1}{r_c}\,\Phi\,\frac{V_{ivo}}{V_{dis}}\left(\frac{P_{exh}}{P_m}\right)^{\frac{1}{k}}}^{\beta} \tag{4}$$

where, r_c indicates the compression ratio; P_{exh} is the exhaust pressure; R is the gas constant, and k is the ratio of specific heats. V_{ivo} is the cylinder volume at IVO moment and V_{dis} is the displacement volume. OF is the valve overlap factor that is calculated by using geometry and timing of both intake and exhaust valves. The parameter C is calculated as:

$$C = \left[1 + \frac{LHV}{c_v\,T_m\left(\frac{m_t}{m_f}\right)r_c^{k-1}}\right]^{\frac{1}{k}} \tag{5}$$

where, LHV represents the lower heating value of the fuel and c_v is the constant-volume specific heat capacity of the in-cylinder gas at the IVC moment. The first term (α) in equation (4) is attributed to the portion of the residual gas caused by the back-flow during the valve overlap period and the second term accounts for the trapped exhaust gases before IVO [52]. As the engine used in this study has a valve overlap period of zero degrees, the first term in equation (4) is assumed to be zero. The value of X_r obtained from equation (4) is used as the starting value in an iterative process to get the final X_r based on calculating the amount of mass retained inside the cylinder at the moment of Exhaust Valve Closing (EVC). This iterative process is detailed later in the section 2.6.

2.1.3 Mixing temperature equation

The T_{ivc} values obtained from equation (2) don't consider the residual gas, so a modified temperature for IVC moment ($T_{ivc,mod}$) is calculated that accounts for the mixing of the fresh charge with the residual gas from the previous cycles. In-cylinder gases are considered as ideal gases and assuming energy is conserved in the mixing process of the residual gas and fresh charge yields:

$$T_{ivc,mod}(i) = (1 - X_r)\left(\frac{c_{v,ch}}{c_{v,t}}\right) T_{ivc}(i) + X_r\left(\frac{c_{v,r}}{c_{v,t}}\right) T_r(i-1) \tag{6}$$

where, i is the cycle number index and subscripts r, ch and t represent the residual gas, the charge (air+fuel+EGR), and the total in-cylinder gas at IVC respectively. Equation (6) suggests a thermal coupling between the cycle (i) and the previous cycle ($i-1$) introduced by residual gases. The c_v properties of different gas components of the in-cylinder mixture

are determined by using the NASA polynomials database [53].

2.1.4 Dilution fraction equation

The amount of residual gas changes the properties and the dilution level of the charge at IVC. This subsequently influences the combustion timing and the fuel burn rate. A parameter is defined as the mixture dilution fraction (X_d) that accounts for the dilution caused by (external) EGR contained in the fresh charge and the dilution caused by the residual gases (internal EGR):

$$X_d = EGR + \frac{X_r}{1 - X_r} \tag{7}$$

since both are present in the engine.

2.2 Compression Stroke (IVC → SOC)

2.2.1 Polytropic compression

Extensive studies for the compression process show that compression of the unburned mixture prior to combustion is approximated by an adiabatic isentropic process and so the compression process is accurately fitted by a polytropic relation ($PV^k = constant$) [5]. Here, blow by is ignored and a polytropic relation is used to calculate the temperature and pressure of the in-cylinder mixture at SOC using the available data at IVC:

$$T_{soc} = T_{ivc,mod} \cdot \left(\frac{V_{ivc}}{V_{soc}}\right)^{k_c - 1} \tag{8}$$

$$P_{soc} = P_{ivc} \cdot \left(\frac{V_{ivc}}{V_{soc}}\right)^{k_c} \tag{9}$$

where, V is the cylinder volume and k_c is the average specific heat capacity ratio for the compression process. The constant $k_c = 1.32$ is chosen based on a best fit on simulated compression results from a TKM [22] for the PRF blends used in this study.

2.2.2 SOC Model

SOC is defined as the point where the third derivative of the pressure trace with respect to the crank angle (θ) in CAD (Crank Angle Degree) exceeds a heuristically determined limit [54]:

$$\left.\frac{d^3P}{d\theta^3}\right|_{ign} = 0.25\frac{\text{bar}}{\text{CAD}^3} \tag{10}$$

A Modified Knock-Integral Model (MKIM) [22] is used to predict SOC. The original Knock Integral Model (KIM) was used to detect knock in SI engines [30]. MKIM adapts the KIM for HCCI combustion using the fact that HCCI combustion has similar chemical kinetics to that of knock in SI engines [36]. MKIM is more practical for control applications, doesn't require any instantaneous in-cylinder parameters, and extends the application of the KIM to the operating conditions with variable dilution and fueling rates. More details of the MKIM can be found in [22]. The MKIM correlation to predict SOC is:

$$\int_{\theta_{ivc}}^{\theta_{soc}} \frac{\Phi^B}{A\ exp\left(\frac{C\left(P_{ivc}\, v_c^{k_c}\right)^D}{T_{ivc,mod}\, v_c^{k_c-1}}\right) N}\, d\theta = 1.0 \tag{11}$$

where, θ is the engine crank angle, B, C, and D are constant parameters. The value of the expression being integrated increases as the point of SOC is approached. A and v_c and

are determined by:

$$v_c(\theta) = \frac{V_{ivc}}{V(\theta)} \quad , \; A = E_1 \, X_d + E_2 \tag{12}$$

where, E_1 and E_2 are constant parameters and the cylinder volume, $V(\theta)$, is calculated at any crank angle using slider crank mechanism [5].

Parameters E_1, E_2, B, C, and D need to be determined to be able to use the MKIM to predict SOC. A similar methodology from [22] is used to parameterize the MKIM where simulation results from a virtual engine [48] at a range of operating conditions are required. To do this the TKM [48] is calibrated for the Ricardo engine described in Table 2. Calibration of the TKM is done by using only 1% of the steady-state experimental points, while the other 99% are used to validate the final model.

Table 2: Configurations of the Ricardo single-cylinder engine

Parameters	**Values**
Bore × Stroke [mm]	80 × 88.9
Compression Ratio	10
Displacement [L]	0.447
Number of Valves	4
IVO, IVC[4] [aBDC]	$-175°$, $55°$
EVO, EVC [aBDC]	$-70°$, $-175°$

The TKM, used to explore the engine variable parameter space, is run over a wide range of engine variables including the engine speed, initial mixture temperature and pressure, EGR rate for the operating conditions listed in Table 3. This results in 10880 TKM simulations

[4]Valve opening/closing point is defined at the valve lift of 0.15 mm. [5]

of which complete ignition occurred in 6554 simulations. Late ignited[5] TKM simulations are excluded since near TDC firing conditions are of practical interest. This results in 5703 TKM simulations that are used to parameterize the MKIM.

Table 3: Parameter variations carried out using the TKM

Variables	**Values**
Engine Speed	800, 1000 rpm
Initial Temperature	80, 85,..., 155, 160 ^{o}C
EGR(%)	0, 10, 20, 30
Equivalence Ratio	0.5, 0.6, 0.7, 0.8
Initial Pressure	95, 100, 105, 110, 115 kPa
Fuel	PRF0, PRF10, PRF20, PRF40
Wall temperature	390 °K

The Nelder-Mead simplex minimization method [55] is used as an off-line optimization technique to parameterize the MKIM using the 5703 TKM simulations. First, parameters B, C, D, and A are determined by applying the estimation code on all the TKM simulation results with four different EGR rates. Then, the parameter A is determined for each group of TKM simulations with the same EGR rate, keeping the values of B, C, and D constant from the first stage. Figure 2 indicates one sample estimation result for the predicted SOC. For all 5703 TKM simulations, the range of average estimation error is from 1.74 to 2.52 CAD and error standard deviation ranges from 1.65 to 1.93 CAD.

[5]TKM simulations in which the second stage of HCCI combustion occurs at the crank angle higher than 15 degrees after Top Dead Center (TDC).

2.3 Combustion Stroke (SOC → EOC)

2.3.1 Fuel burn rate model

Fuel burning rate influences HCCI combustion in terms of efficiency, stability and cyclic variability [10, 9] and should be controlled to achieve desirable HCCI performance. Prediction of SOC is necessary but not sufficient for a model-based control of HCCI combustion since different combustion durations can occur with a same SOC. As the main stage of HCCI combustion has a steep heat release slope, CA50 (the crank angle of 50% fuel burned) is a robust feedback indicator of an HCCI combustion [44]. Thus CA50 (representing both SOC and burn duration) is the main focus in this paper. A simple model used to predict both CA50 and the crank angle for the End of Combustion (θ_{eoc}) is described next. θ_{eoc} is defined as the crank angle where 99% of the fuel mass is burned. A modified Wiebe function [47] is used to predict fuel mass fraction burned (x_b) and to calculate CA50 and θ_{eoc}:

$$x_b(\theta) = 1 - exp\left(-A\left[\frac{\theta - \theta_{soc}}{\theta_d}\right]^B\right) \tag{13}$$

where, A and B are constant parameters and θ_{soc} is SOC crank angle and θ_d is the combustion duration determined by:

$$\theta_d = C\,(1 + X_d)^D\ \Phi^E \tag{14}$$

where, C, D, and E are constant parameters. The fuel burn rate model requires the parameter values of A, B, C, D, and E in order to predict CA50 ($x_b = 0.5$) and θ_{eoc} ($x_b = 0.99$) and the method in [47] is used to parameterize the model. Nelder-Mead simplex minimization method [55] is applied on half of the steady-state experimental data points

to determine the model parameters. The data points are the same as the points used to parameterize the IVC correlations (2.1.1) and conditions of these points are detailed in section 3. The resulting parameters are $A = 2.02$, $B = 5.08$, $C = 5.98$, $D = 0.01$, and $E = -0.02$. By examining these parameters it can be seen that the model predicts CA50 advances and θ_d shortens with an increase in equivalence ratio, but the combustion is prolonged by increasing the dilution rate. This trend is consistent with observations from experimental studies [7, 10].

2.3.2 EOC state equations

During combustion, the combustion chamber is considered as a closed system and the first law of thermodynamics is applied on the system between SOC and EOC to obtain the temperature and pressure of in-cylinder gas at EOC using available properties at SOC:

$$U_{eoc} = U_{soc} + Q_{fuel} - Q_w - W_{soc-eoc} \tag{15}$$

where, U is the internal energy; Q_{fuel} is the energy released from burning fuel; Q_w is the heat loss from the in-cylinder gas to the surrounding walls and $W_{soc-eoc}$ is the work produced during the crank angle interval between SOC and EOC. Q_w is assumed negligible in equation (15) because HCCI combustion is very fast and little time is available for heat transfer and the surface area for heat transfer is also small by having a desirable HCCI combustion occur at crank angles close to TDC [9]. An empirical correlation is obtained from experimental measurements to predict the $W_{soc-eoc}$:

$$W_{soc-eoc} = m_f \; LHV \overbrace{\frac{P_m^A \; N^B}{(1+EGR)^C} \left(D_1 \, \theta_{soc}^2 + D_2 \, \theta_{soc} + D_3\right)}^{\mathbb{W}} \tag{16}$$

where, m_f is the mass of the fuel injected per cycle and A, B, C, D_1, D_2, D_3 are the

constant parameters that are determined by applying Nelder-Mead optimization technique on the half of the steady-state experimental data detailed in the section 3. The resulting parameters are $A = 2.629$, $B = -2.860$, $C = -0.056$, $D_1 = 0.021$, $D_2 = -3.711$, $D_3 = 0.010$. Correlation (16) predicts ignition timing (θ_{soc}) influences the amount of the work produced from an HCCI combustion. This is also observed in the experimental study in [56] where it is shown that ignition timing influences Indicated Mean Effective Pressure (IMEP) in HCCI combustion.

In comparison to the $W_{soc-eoc}$ term in equation (15), the Q_{fuel} term is much larger in magnitude. The energy released from the fuel, Q_{fuel}, is given by:

$$Q_{fuel} = m_f \; . \; CoC \; . \; LHV \tag{17}$$

where, CoC is the Completeness of Combustion. LHV for an arbitrary blend of PRF fuels ($\%V_{_n} + \%V_{_{iso}}$; iso for Isooctane, n for n-Heptane) is evaluated by:

$$LHV = \frac{\%V_{_n}\, \rho_{_n}\, LHV_{_n} \;+\; \%V_{_{iso}}\, \rho_{_{iso}}\, LHV_{_{iso}}}{\%V_{_n}\, \rho_{_n} \;+\; \%V_{_{iso}}\, \rho_{_{iso}}} \tag{18}$$

where, $\%V$ is the volume percentage; ρ is the density of the fuel . CoC in equation (17) is calculated by the following empirical correlation that is parameterized with the same experimental data used for correlation (16):

$$CoC = \frac{\Phi^A \; P_m^B}{(1 + EGR)^C} \left(D_1\, \theta_{soc}^2 + D_2\, \theta_{soc} + D_3 \right) \tag{19}$$

where, $A = 0.169$, $B = 0.165$, $C = 0.053$, $D_1 = -0.001$, $D_2 = 0.458$, $D_3 = 1.390$. The CoC correlation suggests a higher CoC when θ_{soc} occurs at TDC or slightly after TDC, but CoC drops for early and late ignitions. This is consistent with the observation in [57] where

the possibility of partial-burn cycles or misfired cycles in HCCI combustion increases when ignition is late. Furthermore, experimental results in [9] show that cyclic variability of HCCI combustion increases for ignitions that are too early or too late. Cyclic variability influences the instability or misfire limit of an HCCI engine.

Mass fraction (y) for each of the combustion reactants are determined using equations (20) to (22) and the mass fraction of the combustion products are calculated using general reaction equations of PRF blends for a complete, lean combustion [58].

$$y_{a} = \frac{m_{a}}{m_{t}} = \frac{AFR\,(1 - X_{r})\,(1 - EGR)}{AFR + 1} \tag{20}$$

$$y_{egr} = \frac{m_{egr}}{m_{t}} = EGR\;(1 - X_{r}) \tag{21}$$

$$y_{f} = \frac{m_{f}}{m_{t}} = \frac{(1 - X_{r})\,(1 - EGR)}{AFR + 1} \tag{22}$$

where, AFR is the air fuel ratio of the charge. Combustion reactants (PRF blend fuel, air, EGR, residual gas) and combustion products (H_2O, CO_2, N_2, O_2) are assumed to be ideal gases. Using this assumption, equations (15) and (16) are combined and rearranged to give the in-cylinder gas temperature at EOC:

$$T_{eoc} = \frac{\left(\sum_{i} c_{v,i}\; y_{i}\right)_{R} .\; T_{soc} + \frac{m_{f}}{m_{t}} .\; LHV\,(CoC - \mathbb{W})}{\left(\sum_{i} c_{v,i}\; y_{i}\right)_{P}} \tag{23}$$

where, symbols R and P stand for Reactants and Products respectively. Finally, pressure at EOC is calculated by using the ideal gas state equation for EOC and IVC conditions assuming constant mass (no blow-by):

$$P_{eoc} = P_{ivc} \cdot \frac{V_{ivc}}{V_{eoc}} \cdot \frac{T_{eoc}}{T_{ivc}} \cdot \frac{R_{eoc}}{R_{ivc}} \tag{24}$$

2.4 Expansion Stroke (EOC → EVO)

2.4.1 Polytropic expansion

Similar to the compression stroke, the expansion of burned gases after EOC can be considered as an adiabatic isentropic process characterized by a polytropic relation [5]. Here, temperature and pressure of the burned gas at Exhaust Valve Opening (EVO) are calculated based on available data from EOC by using a polytropic relation:

$$T_{evo} = T_{eoc} \cdot \left(\frac{V_{eoc}}{V_{evo}}\right)^{k_e - 1} \tag{25}$$

$$P_{evo} = P_{eoc} \cdot \left(\frac{V_{eoc}}{V_{evo}}\right)^{k_e} \tag{26}$$

where, k_e is the average specific heat capacity ratio for the expansion process that can be determined with a similar approach to section 2.2.1.

2.5 Exhaust Stroke (EVO → EVC)

2.5.1 Exhaust gas model

When the exhaust valves open, the in-cylinder gas goes through a blow-down phase to a gas displacement phase from the moving piston. A single zone crank-angle resolved model is developed to predict the gas state (temperature, pressure, mass) at the EVC moment. A quasi-steady assumption is used and the properties of the gas including the gas leaving or entering into the cylinder are assumed steady and homogeneous. Furthermore, the change in the kinetic and potential energies of the gas is ignored. Using these assumptions, the first

law of thermodynamics for the exhaust gas as an open Control Volume (CV) between the state "1" and the state "2" yields:

$$\dot{Q}_w - \dot{W} = \sum \dot{m}_{ce} h_{ce} + \left[\frac{(m_2 u_2 - m_1 u_1)_{CV}}{\Delta t} \right] - \sum \dot{m}_{ec} h_{ec} \tag{27}$$

where, h is the enthalpy of the gas and Δt is the time span between states "1" and "2". Index "*ce*" refers to the exhaust flow from the cylinder to the exhaust manifold and "*ec*" refers to the backflow from the exhaust manifold to the cylinder. As the Ricardo engine has a zero valve overlap period, small exhaust backflow is expected and no flow between the intake manifold and the cylinder is considered during the exhaust stroke.

The heat transfer to the cylinder walls is modeled using the Modified Woschni heat transfer correlation that is adopted for HCCI engines [59]:

$$\dot{Q_w}(t) = -h_c(t)\, A_s\, (T_g - T_w) \tag{28}$$

where, A_s is the in-cylinder surface area; T_g and T_w are gas temperature and average wall temperature; h_c is the convective heat transfer coefficient that is given by:

$$h_c(t) = \alpha_{scaling} \;.\; L(t)^{-0.2}.\; P(t)^{0.8}.\; T(t)^{-0.73}.\; \left(2.28\, \bar{S}_p\right)^{0.8} \tag{29}$$

where, L is the instantaneous cylinder height; P and T are the gas temperature and pressure; $\bar{S}_p$ is the average piston speed. $\alpha_{scaling}$ is the scaling factor that is used to tune the correlation to match a specific engine geometry [59]. The value of $\alpha_{scaling} = 2.0$ is chosen using the simulation results from [60].

Equation (27) is rearranged by using the ideal gas assumption and generated work equation ($\dot{W} = -P\dot{V}$). T_{evc} is determined from EVO to EVC using the following equation in the combination with ideal gas state equation

$$T_2 = \frac{T_1 \left(\sum_i m_{i,1}\ c_{v_i,1} - \sum_i c_{p_i,1} \left(m_{i,ce} + m_{i,ec}\right)\right) + Q_w + P_1\, dV}{\sum_i m_{i,2}\ c_{v_i,2}} \tag{30}$$

and exhaust valve flow model.

2.5.2 Exhaust valve flow model

The flow across the exhaust valves is modeled by using the orifice equation for one-dimensional, steady-state, compressible, isentropic flow [5]:

$$\dot{m} = \begin{cases} \frac{C_D\, A_R\, P_o}{\sqrt{R\, T_o}} \left(\frac{P_T}{P_o}\right)^{\frac{1}{k}} \left\{ \frac{2\,k}{k-1} \left[1 - \left(\frac{P_T}{P_o}\right)^{\frac{k-1}{k}} \right] \right\}^{\frac{1}{2}}, & \text{if} \quad P_T/P_o > [2/(k+1)]^{k/(k-1)} \quad \text{(a)} \\ \frac{C_D\, A_R\, P_o}{\sqrt{R\, T_o}}\ k^{\frac{1}{2}} \left(\frac{2}{k+1}\right)^{\frac{k+1}{2(k-1)}}, & \text{otherwise} \quad \text{(b)} \end{cases} \tag{31}$$

where, C_D is the discharge coefficient; subscripts "$_o$" and "$_T$" refer to the gas properties at the upstream and the downstream of the exhaust valves. A_R is a reference area (called curtain area) which is calculated by:

$$A_R = \pi\, d_v\, L_v \tag{32}$$

where, d_v is the diameter of the exhaust valves ($d_v = 27mm$) and L_v is the axial valve lift that is measured off-line. Figure 3 shows the measured lift profile for the valves. C_D is experimentally determined using flow measurements on a flow-bench apparatus for a similar cylinder-head. Flow measurements are done at 45 different valve lifts and pressure ratios (P_T/P_o) while sweeping from choked-flow conditions ($P_T/P_o \leq [2/(k+1)]^{k/(k-1)}$) to the un-choked-flow conditions [5]. The following correlation is found to work well on the available data:

$$C_{_D} = A + B\ Ln\left(\frac{L_v}{d_v}\right) + C\ \left(Ln\left(\frac{L_v}{d_v}\right)\right)^2 + D\ Ln\left(\frac{P_o}{P_T}\right) \tag{33}$$

where, A = -0.152, B = -0.577, C = -0.082, and D = 0.294. For the 45 flow measurements, the average error and standard deviation error of predicted $C_{_D}$ from correlation (33) are 0.02 and 0.03 respectively.

2.5.3 Residual gas state

In-cylinder gas temperature and the retained mass inside the cylinder at the moment of EVC determine the temperature of residual gas (T_r) and the mass fraction of the residual gas (X_r).

2.6 Final Model Layout

A structure of a dynamic full-cycle simulation model has been formed that includes thermal coupling from one cycle to the next cycle through mass and thermal properties of residual gases. Figure 4 shows an overall schematic of the model programmed in Matlab computing environment. The model requires seven measurable inputs including intake temperature, intake pressure, EGR, engine speed, equivalence ratio, mass of injected fuel, and pressure in the exhaust port.

Three iteration loops are needed in the model (see Figure 4) with the first two loops used to get the initial X_r in the intake stroke and to get T_{eoc} in the combustion stroke. These two loops are present due to the dependance of the gas specific heat capacity (c_v) on X_r and gas temperature, but X_r and T_{eoc} depend on c_v in equation (5) and equation (23). Figure 5 shows a sample simulation result of the iterative process in the model to predict T_{eoc}. It can be seen the simulation converges to a constant value with a small error ($< 1°$C) within seven

iterations. Four to six iterations are typically required to get T_{eoc} within 5°C resolution for different simulation conditions. The third iteration loop in the model (Figure 4) calculates the X_r. The initial X_r value from equation (4) is tested at the end of simulation cycle (EVC) and then based on the difference between the initial and calculated values, iteration is performed by repeating the simulation from IVC to EVC. This process continues until consecutive values of X_r converge within a tolerance. However, for each operating point this iterative process is run only once for the first cycle to get the correct X_r, then the values of X_r for the next cycle is always determined from calculated X_r of the previous cycle. Figure 6 indicates a sample simulation result of the iterative process to get correct X_r for the first cycle of a new operating point. As seen in the figure, X_r converges to 6.7% $\pm$ 0.01% within 10 iterations from the starting value of 2.2% obtained from equation (4). Typically five to seven iterations are required to obtain X_r with a convergence error of 0.001 for different simulation conditions.

3 Experimental Engine Setup

Experimental data is collected using a single-cylinder Ricardo Mark III engine with Rover K7 head. The Ricardo engine has a combustion chamber with pent-roof design with a centrally located spark plug and it uses a flat top cast aluminum piston with valve reliefs. Dual camshafts located in the cylinder head operate two intake and two exhaust valves. Table 2 indicates the timing of the valves as well as the geometrical specification of the engine.

An experimental setup schematic is shown in Figure 7. Two separate fuel systems with 3-bar fuel pressure are used to ensure injection on closed intake valves. One fuel system is

used to inject n-Heptane and the other is used to inject Isooctane. The separate flow rate control of each of these two fuels allows any desired PRF octane number to be obtained. Each system consists of a fuel tank, fuel pump, fuel pressure regulator, and fuel injector. Both n-Heptane and Isooctane injectors are aimed directly at the back of the intake valves and they are located respectively at the approximate position of $10\,cm$ and $25\,cm$ from the intake valves. The fresh intake air entering the engine is first passed through a laminar air-flow meter for flow rate measurement. Then, the fresh charge is mixed with recirculated hot exhaust gases (EGR) using an insulated return line from the exhaust to the intake manifold. Next, a supercharger driven by a variable speed electric motor adjusts the intake manifold pressure and then a 600W electrical band-type heater sets the mixture temperature to a desired value using a closed-loop controller. Finally the exhaust gases exiting the cylinder are sampled for emission analysis. As shown in Figure 7, the emission can be sampled from either the intake manifold or from the exhaust manifold.

The engine out AFR value is measured by ECM AFRecorder 1200 UEGO positioned approximately 25cm downstream of the exhaust valves. Intake temperature is measured with a K-type thermocouple positioned in the intake manifold before the charge entering into the cylinder. The EGR rate is determined by comparing the CO_2 concentrations in the intake and exhaust manifolds, and by assuming that all CO_2 in the intake manifold is from the exhaust gases. Measurement of the cylinder pressure is done using a Kistler water-cooled ThermoCOMP (model 6043A60) piezoelectric pressure sensor that is flush mounted in the cylinder head. Crank angle measurement with 0.1^o resolution, is done using a BEI optical encoder connected to the crankshaft on the front of the engine. A dSpace MicroAutobox

1401/1501 ECU is used to control the injection Pulse Width (PW) of n-Heptane and Isooctane injectors to provide the desired AFR and Octane Number (ON). Injected fuel mass per cycle ($m_{f,i}$) for both injectors is estimated from the PW of the injectors [61]:

$$m_{f,inj}\left[\frac{g}{cycle}\right] = C_f \ . \ PW_{inj}\,[ms] + C_{offset} \tag{34}$$

where, C_f and C_{offset} are constant parameters that are determined by injector calibration from steady state fuel flow measurements at different operating conditions. The resulting C_f and C_{offset} are 3.30 $\left[\frac{g}{ms.cycle}\right]$ and -2.90 $\left[\frac{g}{cycle}\right]$ for Isooctane injector and 2.95 $\left[\frac{g}{ms.cycle}\right]$ and -2.74 $\left[\frac{g}{cycle}\right]$ for n-Heptane injector. Details of the procedure to calculate these parameters are explained in the [62].

The Ricardo engine is run to collect two types of experiment measurements: steady-state points, transient points. Table 5 details the experimental conditions of 149 steady-state points used in this study. The **steady-state** data points are used to parameterize the model and to validate the model for steady operation. Table 5 shows the engine operating conditions of the steady-state data points used to parameterize empirical models in this study. The low compression ratio of the Ricardo engine makes HCCI operation occur only for lower ON fuels and at lower engine speeds. PRF40 for the Ricardo engine is the highest PRF for which HCCI operation is possible for a range of loads. For each steady-state test point, pressure traces from 200 consecutive engine cycles with 0.1 CAD resolution are recorded. Due to amplification of high frequency noise when numerically differentiating the pressure trace to get SOC based on equation (10), a second order Butterworth low pass filter with cutoff frequency of $f_c = 0.556\text{CAD}^{-1}$ is applied to the experimental pressure signal. The

pressure signal is filtered in the crank angle domain to maintain a constant crank angle cutoff frequency for different engine speeds, filtering was done in both forward and reverse directions to avoid any phase shift incurred by the filtering process. Pressure trace data is used with Rassweiler method [63] to calculate fuel mass fraction burnt parameters such as CA50.

Table 4: Engine's steady-state operating conditions (149 points)

Variables	**Values**
Fuel	PRF0, PRF10, PRF20, PRF40
Engine Speed [rpm]	800 - 1000
Manifold Temperature [^oC]	60 - 152
EGR [%]	0 - 28.5
Equivalence Ratio	0.29 - 0.94
Manifold Pressure [kPa]	89 - 156.6
Coolant/Oil Temperature [^oC]	70 - 80

Table 5: Steady-state engine operating conditions for the data points used to parameterize the empirical models in Sections 2.1.1, 2.3.1, and 2.3.2. (74 points)

Variables	**Values**
Fuel	PRF0, PRF10, PRF20, PRF40
Engine Speed [rpm]	800 - 1000
Manifold Temperature [^oC]	70 - 152
EGR [%]	0 - 27
Equivalence Ratio	0.29 - 0.94
Manifold Pressure [kPa]	89 - 145
Coolant/Oil Temperature [^oC]	70 - 80

Transient experiments are performed by transient fueling at a constant air flow rate.

Fuel injection pulse width is open loop scheduled by the ECU to achieve desired Φ and ON. Fuel mass flow rate are first stepped up and then stepped down to the initial value to study the system dynamics in both directions of increasing and decreasing engine loads. During each transient test 450 cycles of cylinder pressure data are recorded at 0.1 CAD and other measured engine variables are recorded at 100Hz.

4 Model Validation

The physics based Control Oriented Model (COM) is validated with over 150 different steady-state and transient experimental test points collected from the Ricardo engine. The validation is done for CA50 values as the best indication of HCCI combustion timing. However, CA50 predictions can be used to estimate other parameters of HCCI combustion timing. For example a strong linear correlation between CA50 and the crank angle of maximum peak pressure (the indicator of combustion stability) is seen in [9] and CA50 also correlates well with SOC and the crank angle of maximum heat release rate for the Ricardo engine. Thus CA50 is an important HCCI engine metric. First the model is validated by steady-state experiments. This predominantly evaluates the performance of the SOC sub-model (2.2.2) and fuel burn rate sub-model (2.3.1) that are parameterized from averaged steady-state data. Then, the remaining validation is done using transient data that evaluates the model for both steady-state operation and the dynamics occurring during transients.

4.1 Steady-state operation

Figure 8 shows a comparison between predicted CA50 with those of experiments for four different fuels at various operating conditions at 800 rpm and 1000 rpm. As the experimental

HCCI data has cyclic variations in CA50, the range of CA50 variation from 200 consecutive cycles for each operating point is also shown in Figure 8. The diamond symbol indicates the average experimental CA50 calculated from averaging the CA50s from 200 cycles and the round symbol shows the predicted CA50 from the model for using the average experimental conditions over 200 cycles for each test point. The average error value shown in the figure is the error between diamond symbols and round symbols. Figure 8 shows a good agreement between the model prediction and the measured experimental CA50. The total average error for 150 steady-state operating points in Figure 8 is 1.26 CAD and the model predictions are usually within the CA50 experimental range. The total average error from the range of experimentally calculated CA50s is 0.16 CAD. To calculate this term, no error is considered when predicted CA50s are within the range of CA50s of individual cycles for each experimental point.

Figure 8 also shows that cyclic variations of CA50 are higher when CA50 occurs late. This is consistent with the observations in previous studies [9, 10]. The position of CA50 highly affects cyclic variations of IMEP and CA50 also influences maximum pressure rise rate characterizing the knock limit [10]. Too late ignitions can misfire while too early ignitions can knock. Therefore only an appropriate window of CA50 provides acceptable HCCI operation. The experimental data shows that acceptable operation in terms of cyclic variations, IMEP and knocking level occurs when CA50 is between 4 and 12 CAD aTDC.

Steady-state CA50 predictions agree well with experimental CA50 measurements considering that SOC model was parameterized using the TKM simulation model and then validated with HCCI experiments of which only 1% of them are used to calibrate the TKM.

As the TKM does not exactly represent the real engine, the error of TKM can be one possible source of error. Other possible sources of error are the inherent error of the applied semi-empirical correlations and neglecting the variation of coolant temperature in the TKM since a constant wall temperature is assumed despite the variation in coolant temperature (Table 5) in the HCCI experiments.

4.2 Transient operation

Transient tests caused by variations in fueling (Φ and ON) are used to validate the model. Variation of Φ and switching of octane number are selected for transient experiments since sensitivity analysis [60] for the current experimental setup suggests to use the octane number and equivalence ratio as the main variables to control HCCI combustion timing for the Ricardo engine.

Figures 9 and 10 show the transient response during the fuel and ON steps. As expected CA50 advances with increasing equivalence ratio, but it retards with increasing octane number. Values of fuel mass flow rate are calculated from injector pulse width from equation (34). Figure 9 compares the predicted system transient response with that of the experiment when equivalence ratio is changed. The figure shows the model captures the overall dynamic trend of changes and predicts CA50 within 1.5 CAD error from those of the experimental data. A limited range of Φ is possible at each constant EGR rate operating point and this range becomes smaller when switching to the fuels with higher octane numbers. Figure 9 shows a step change in fueling rate is commanded to the fuel injectors though this sudden change is not seen in the measured Φ values due to fuel transport dynamics from the intake port to the cylinder. Fuel transport dynamics consist of depositing the injected fuel into the

fuel puddle at the intake port walls and the dynamics of evaporation of both fuel film and airborne fuel droplets. The fuel transport dynamics causes Φ excursions seen in Figures 9 and 10.

Figure 10 and Figure 11 compare predicted CA50 from the model with those of the experiment when ON is switched from 0 to 20. Transient response of the engine is shown for: only ON change in Figure 10; and simultaneous change of ON with Φ in Figure 11. For the experimental conditions tested a step change of 20 in fuel octane number at a constant Φ often violated knock/mis-fire limits of HCCI combustion. The combination of ON and Φ is expectant to achieve the desirable ignition timing. Good agreement between predicted and experimental CA50 during these step transients is seen in Figures 10 and 11. In Figures 10 and 11 the model response of CA50 to the input step occurs earlier than in the real engine. This is attributed to the unmodeled fuel transport dynamics. This effect is stronger in Figure 11 where fueling changes are influenced by both ON change and Φ change.

5 Summary and Future Work

A physics based Control Oriented Model (COM) having HCCI combustion timing (CA50) as the output has been developed. The seven inputs of the model are: intake pressure, intake temperature, EGR rate, equivalence ratio, exhaust pressure and amount of fuel injected. All of these inputs can be relatively easily measured or estimated on an engine.

Over a wide range of conditions a more complex and computationally intensive TKM model is used to parameterize the COM. The COM is cross validated with 150 transient and steady-state experimental measurements. In steady-state the average error between the model and experimental measurements for combustion phasing is less than 1.5 CAD. This

error seems an acceptable compromise between computation and accuracy. For this engine an 8 degree window of CA50, between 4 – 12 CAD aTDC is found to provide stable HCCI operation with values higher than this tending to have high cycle-to-cycle variation.

Three types of rectangular transients are simulated with the COM and compared to experimental results. In all cases the experimental inputs are used in the "open loop" simulation with no correction from the measured output. A step in equivalence ratio (by varying the fueling quantity), a step in octane number and a simultaneous combination of these two are the three transient tests performed. Comparing to the experimental measurements the simulation seems to capture the transient dynamics with a constant offset.

The COM from this work can be used as a simulation bed to design the HCCI combustion controller. Future work includes utilizing the COM for controller design and also modifying the COM for on-line model-based HCCI control. In addition, the COM can be improved by including the thermal transient dynamics for the conditions with variable coolant temperatures. A more detailed gas exchange dynamic model may be required for the cases where variable valve timing is used as a control variable to achieve desired HCCI ignition timing.

Acknowledgements

The authors graciously acknowledge the Natural Sciences and Engineering Research Council of Canada (NSERC), AUTO21 Network of Centers of Excellence, WestGrid and Daimler for supporting this work. For their contributions in collecting the experimental data A. Audet and R. Lupul are gratefully acknowledged.

References

[1] Zhao, H., 2007, *Homogeneous Charge Compression Ignition (HCCI) and Controlled Auto Ignition (CAI) Engines for the Automotive Industry*, Woodhead Publishing Limited, Brunel University.

[2] Zhao, F., Asmus, T. W., Assanis, D. N., Dec, J. E., Eng, J. A., and Najt, P. M., 2003, *Homogeneous Charge Compression Ignition (HCCI) Engines*, SAE Publication PT-94.

[3] Aleiferis, P. G., Charalambides, A. G., Hardalupas, Y., Taylor, A. M. K. P., and Urata, Y., 2006, "Autoignition Initiation and Development of n-Heptane HCCI Combustion Assisted by Inlet Air Heating, Internal EGR or Spark Discharge: An Optical Investigation," SAE Paper No. 2006-01-3273.

[4] Onishi, S., Jo, S. H., Shoda, K., Jo, P. D., and Kato, S., 1979, "Active Thermo-Atmosphere Combustion (ATAC) A New Combustion Process for Internal Combustion Engines," SAE Paper No. 790501.

[5] Heywood, J. B., 1988, *Internal Combustion Engine Fundamentals*, McGraw-Hill, New York.

[6] Stanglmaier, R. H. and Roberts, C. E., 1999, "Homogeneous Charge Compression Ignition (HCCI): Benefits, Compromises, and Future Engine Applications," SAE Paper No. 1999-01-3682.

[7] Lu, X., Chen, W., Hou, Y., and Huang, Z., 2005, "Study on the Ignition, Combustion and Emissions of HCCI Combustion Engines Fueled With Primary Reference Fuels," SAE Paper No. 2005-01-0155.

[8] Yao, M., Zheng, Z., Zhang, B., and Chen, Z., 2004, "The Effect of PRF Fuel Octane Number on HCCI Operation," SAE Paper No. 2004-01-2992.

[9] Shahbakhti, M., Lupul, R., and Koch, C. R., 2007, "Cyclic Variations of Ignition Timing in an HCCI Engine," Proceeding of ASME/IEEE Joint Rail Conference & Internal Combustion Engine Spring Technical Conference.

[10] Kalghatgi, G. T. and Head, R. A., 2006, "Combustion Limits and Efficiency in a Homogeneous Charge Compression Ignition Engine," Int. Journal of Engine Research, **7**, pp. 215–236.

[11] Santoso, H., Matthews, J., and Cheng, W. K., 2005, "Managing SI/HCCI Dual-Mode Engine Operation," SAE Paper No. 2005-01-0162.

[12] Midlam-Mohler, S., Haas, S., Guezennec, Y., Bargende, M., and Rizzoni, G., 2004, "Mixed-Mode Diesel HCCI/DI With External Mixture Preparation," SAE Paper No. 2004-05-0446.

[13] Shaver, G. M., Roelle, M. J., and Gerdes, J. C., 2006, "Modeling Cycle to Cycle Dynamics and Mode Transition in HCCI Engines with Variable Valve Actuation," Journal of Control Engineering Practice, **14**, pp. 213–222.

[14] Xingcai, L., Yuchum, H., Libin, J., Linlin, Z., and Zhen, H., 2006, "Heat Release Analysis on Combustion and Parametric Study on Emissions of HCCI Engines Fueled with 2-Propanol/n-Heptane Blend Fuels," Journal of Energy & Fuel, pp. 1870–1878.

[15] Koopmans, L., Backlund, O., and Denbratt, I., 2002, "Cycle to Cycle Variations: Their Influence on Cycle Resolved Gas Temperature and Unburned Hydrocarbons from a Camless Gasoline Compression Ignition Engine," SAE Paper No. 2002-01-0110.

[16] Kong, S. C. and Reitz, R. D., 2003, "Numerical Study of Premixed HCCI Engine Combustion and its Sensitivity to Computational Mesh and Model Uncertainties," Combustion Theory and Modeling, pp. 417–433.

[17] Aceves, S. M., Flowers, D. L., Westbrook, C. K., Smith, J. R., Pitz, W., Dibble, R., Christensen, M., and Johansson, B., 2000, "A Multi-zone Model for Prediction of HCCI Combustion and Emissions," SAE Paper No. 2000-01-0327.

[18] Kongsereeparp, P., Checkel, M. D., and Kashani, B., 2005, "A Stand-alone Multi-Zone Model for Combustion in HCCI Engines," ASME Internal Combustion Engine Division 2005 Fall Technical Conference.

[19] Aceves, S. M., Flowers, D. L., Martinez-Frias, J., Smith, J. R., Dibble, R., Au, M., and Girard, J., 2001, "HCCI Combustion: Analysis and Experiments," SAE Paper No. 2001-01-2077.

[20] Fiveland, S. B. and Assanis, D. N., 2000, "A Four-stroke Homogeneous Charge Compression Ignition Engine Simulation for Combustion and Performance Studies," SAE Paper No. 2000-01-0332.

[21] Millet, J. B., Maroteaux, F., Emery, P., and Sorine, M., 2006, "A Reduced Model of HCCI Combustion in View of Application to Model-Based Engine Control Systems," SAE Paper No. 2006-01-3297.

[22] Swan, K., Shahbakhti, M., and Koch, C. R., 2006, "Predicting Start of Combustion Using a Modified Knock Integral Method for an HCCI Engine," SAE Paper No. 2006-01-1086.

[23] Canova, M., Garzarella, L., Ghisolfi, M., M., M. S., Y., G., and G., R., 2005, "A Control-Oriented Mean-Value Model for HCCI Diesel Engines with External Mixture Formation," Proceedings of IMECE2005, ASME International Mechanical Engineering Congress.

[24] Shaver, G. M., Gerdes, J. C., Roelle, M. J., Caton, P. A., and Edwards, C. F., 2005, "Dynamic Modeling of Residual-Affected Homogeneous Charge Compression Ignition Engines with Variable Valve Actuation," ASME Journal of Dynamic Systems, Measurement and Control, **127**, pp. 374–381.

[25] Halstead, M., Kirsch, L., and Keck, J., 1977, "The Autoignition of Hydrocarbon Fuels at High Temperatures and Pressures-Fitting of a Mathematical Model," Combustion and Flame, **30**, pp. 45–60.

[26] Bengtsson, J., Gafvert, M., and Strandh, P., 2004, "Modeling of HCCI Engine Combustion for Control Analysis," Proceeding of IEEE conference on decision and control, pp. 1682–1687.

[27] Karagiorgis, S., Collings, N., Glover, K., and Petridis, T., 2006, "Dynamic Modeling of Combustion and Gas Exchange Processes for Controlled Auto-Ignition Engines," Proceeding of the 2006 American Control Conference, minneapolis, Minnesota, USA, June 14-16.

[28] Shaver, G. M., Roelle, M. J., Caton, P. A., Kaahaaina, N. B., Ravi, N., Hathout, J., Ahmed, J., Kojic, A., Park, S., Edwards, C. F., and Gerdes, J. C., 2005, "A Physics-Based Approach to the Control of Homogeneous Charge Compression Ignition Engines with Variable Valve Actuation," International Journal of Engine Research, **6**, pp. 361–375.

[29] Rausen, D. J., Stefanopoulou, A. G., Kang, J.-M., Eng, J. A., and Kuo, W., 2004, "A Mean-Value Model for Control of Homogeneous Charge Compression Ignition (HCCI) Engines," Proceeding of American Control Conference, pp. 125–131.

[30] Livengood, J. C. and Wu, P. C., 1955, "Correlation of Autoignition Phenomena in Internal Combustion Engines and Rapid Compression Machines," Fifth Symposium (International) on Combustion, pp. 347–356.

[31] Agrell, F., Angstrom, H. E., Eriksson, B., Wikander, J., and Linderyd, J., 2003, "Integrated Simulation and Engine Test of Closed Loop HCCI Control by Aid of Variable Valve Timings," SAE Paper No. 2003-01-0748.

[32] Ohyama, Y., 2001, "Engine Control Using a Real-Time Combustion Model," SAE paper No. 2001-01-0256.

[33] Iida, M., Aroonsrisopon, T., Hayashi, M., Foster, D., and Martin, J., 2001, "The Effect of Intake Air Temperature, Compression Ratio and Coolant Temperature on the Start of Heat Release in an HCCI Engine," SAE Paper No. 2001-01-1880.

[34] Souder, J. S., Mehresh, P., Hedrick, J. K., and Dibble, R. W., 2004, "A Multi-Cylinder HCCI Engine Model for Control," Proceedings of IMECE2004, pp. 307–316.

[35] Ohyama, Y., 2000, "Engine Control Using Combustion Model," SAE paper No. 2000-01-0198.

[36] Chiang, C. J. and Stefanopoulou, A. G., 2006, "Sensitivity Analysis of Combustion Timing and Duration of Homogeneous Charge Compression Ignition (HCCI) Engines," Proceeding of the 2006 American Control Conference, minneapolis, Minnesota, USA, June 14-16.

[37] Shaver, G. M., Roelle, M. J., and Gerdes, J. C., 2009, "Physics-based Modeling and Control of Residual-Affected HCCI Engines," Journal of Dynamic Systems, Measurement and Control, **131**, Issue 2.

[38] Chiang, C. J. and Stefanopoulou, A. G., 2007, "Stability Analysis in Homogeneous Charge Compression Ignition (HCCI) Engines With High Dilution," IEEE Transactions on Control Systems Technology, **15**, pp. 209–219.

[39] Killingsworthy, N. J., Acevesz, S. M., Flowersz, D. L., and Krsti, M., 2006, "A Simple HCCI Engine Model for Control," IEEE International Conference on Control Applications.

[40] Bengtsson, J., Strandh, P., Johansson, R., Tunesta, P., and Johansson, B., 2007, "Hybrid Modelling Of Homogeneous Charge Compression Ignition (HCCI) Engine Dynamics - A Survey," International Journal of Control, **80**, pp. 1814–1847.

[41] Pfeiffer, R., Haraldsson, G., Olsson, J. O., Tunestal, P., Johansson, R., and Johansson, B., 2004, "System Identification and LQG Control of Variable-Compression HCCI Engine Dynamics," Proceeding of IEEE International Conference on Control Applications, pp. 1442–1447.

[42] Wagner, R. M., Edwards, K. D., Daw, C. S., Jr., J. B. G., and Bunting, B. G., 2006, "On the Nature of Cyclic Dispersion in Spark Assisted HCCI Combustion," SAE Paper No. 2006-01-0418.

[43] Daw, C. S., Wagner, R. M., Edwards, K. D., and Jr., J. B. G., 2007, "Understanding the Transition Between Conventional Spark-Ignited Combustion and HCCI in a Gasoline Engine," Proceedings of the Combustion Institute, **31**, pp. 2887–2894.

[44] Bengtsson, J., Strandh, P., Johansson, R., Tunesta, P., and Johansson, B., 2004, "Closed-Loop Combustion Control Of Homogeneous Charge Compression Ignition (HCCI) Engine Dynamics," International Journal of Adaptive Control and Signal Processing, **18**, pp. 167–179.

[45] Bengtsson, J., Strandh, P., Johansson, R., Tunesta, P., and Johansson, B., 2006, "Hybrid Control Of Homogeneous Charge Compression Ignition (HCCI) Engine Dynamics," International Journal of Control, **79**, pp. 422–448.

[46] Shahbakhti, M., Lupul, R., and Koch, C. R., 2007, "Predicting HCCI Auto-Ignition Timing by Extending a Modified Knock-Integral Method," SAE Paper No. 2007-01-0222.

[47] Shahbakhti, M. and Koch, C. R., 2007, "Control Oriented Modeling of Combustion Phasing for an HCCI Engine," Proceeding of American Control Conference.

[48] Kirchen, P., Shahbakhti, M., and Koch, C. R., 2007, "A Skeletal Kinetic Mechanism for PRF Combustion in HCCI Engines," Journal of Combustion Science and Technology, **179**, pp. 1059–1083.

[49] Shahbakhti, M., Lupul, R., and Koch, C. R., 2007, "Sensitivity Analysis and Modeling of HCCI Auto-Ignition Timing," Proceeding of the Fifth IFAC Symposium on Advances in Automotive Control, pp. 303 – 310.

[50] Zhao, H., Peng, Z., Williams, J., and Ladommatos, N., 2001, "Understanding the Effects of Recycled Burnt Gases on the Controlled Autoignition (CAI) Combustion in Four-Stroke Gasoline Engines," SAE Paper No. 2001-01-3607.

[51] Karagiorgis, S., Collings, N., Glover, K., Coghlan, N., and Petridis, A., 2006, "Residual Gas Fraction Measurement and Estimation on a Homogeneous Charge Compression Ignition Engine Utilizing the Negative Valve Overlap Strategy," SAE Paper No. 2006-01-3276.

[52] Cavina, N., Siviero, C., and Suglia, C., 2004, "Residual Gas Fraction Estimation: Application to a GDI Engine With Variable Valve Timing and EGR," SAE Paper No. 2004-01-2943.

[53] Burcat, A., 2001, "Third Millenium Ideal Gas and Condensed Phase Thermochemical Database for Combustion," Tech. Rep. TAE 867, Faculty of Aerospace Engineering, Israel Institute of Technology, ftp.technion.ac.il/pub/supported/aetdd/thermodynamics.

[54] Checkel, M. D. and Dale, J. D., 1986, "Computerized Knock Detection from Engine Pressure Records," SAE Paper No. 860028.

[55] Nelder, J. A. and Mead, R., 1965, "A Simplex Method for Function Minimization," Computer Journal, pp. 308–313.

[56] Xingcai, L., Libin, J., Junjun, M., and Zhen, H., 2007, "Combustion Stability and Cycle-by-Cycle Variations of n-Heptane Homogeneous Charge Compression Ignition Combustion," Journal of Energy & Fuel, **21**, pp. 1468–1473.

[57] Sjoberg, M. and Dec, J. E., 2007, "Comparing Late-Cycle Autoignition Stability for Single- and Two-Stage Ignition Fuels in HCCI Engines," Proceedings of the Combustion Institute, **31**, pp. 2895–2902.

[58] Turns, S. R., 2000, *An Introduction to Combustion: Concepts and Applications*, McGraw-Hill, 2nd ed.

[59] Chang, J., Guralp, O., Filipi, Z., Assanis, D., Kuo, T., Najt, P., and Rask, R., 2004, "New Heat Transfer Correlation for an HCCI Engine Derived From Measurements of Instantaneous Surface Heat Flux," SAE Paper No. 2004-01-2996.

[60] Shahbakhti, M. and Koch, C. R., 2007, "Thermo-Kinetic Combustion Modeling of an HCCI Engine to Analyze Ignition Timing for Control Applications," Proceeding of Combustion Institute/Canadian Section (CI/CS) Spring Technical Conference.

[61] Moskwa, J. J., 1988, *Automotive Engine Modeling for Real-Time Control*, Ph.D. Thesis, Massachusetts Institute of Technology.

[62] Lupul, R., 2008, *Steady State and Transient Characterization of a HCCI Engine with Varying Octane Fuel*, M.Sc. thesis, University of Alberta.

[63] Rassweiler, G. M. and Withrow, L., 1938, "Motion Pictures of Engine Flames Correlated with Pressure Cards," SAE Transactions, **42**, pp. 185–204.

Figures

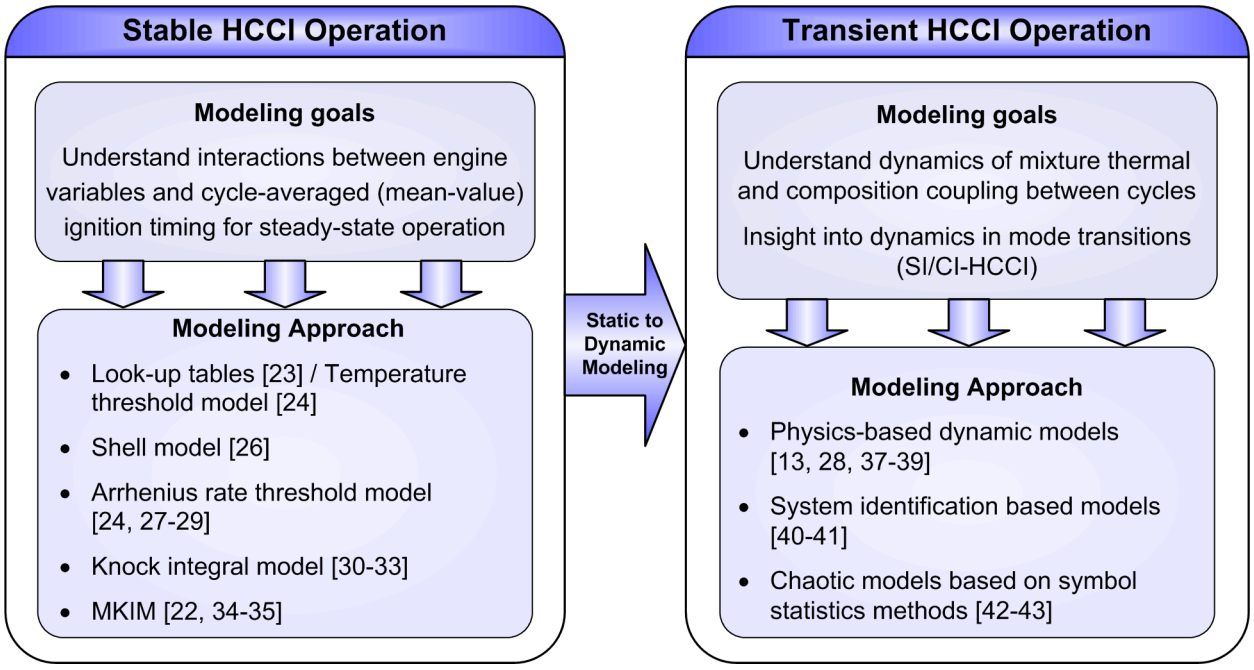

Figure 1: Main modeling approaches to predict HCCI combustion timing for control applications.

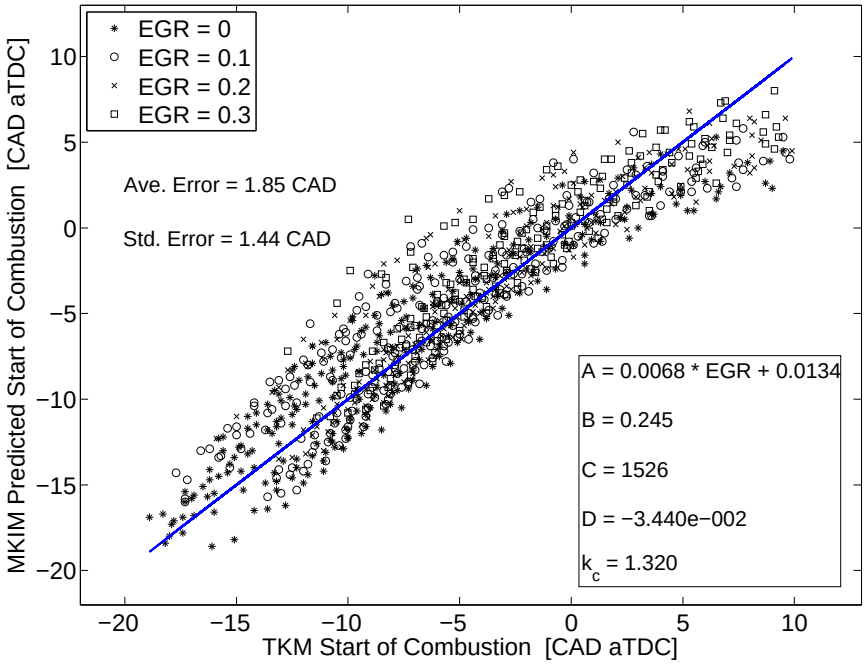

Figure 2: MKIM predicted SOC versus TKM simulations at various engine conditions at 800 rpm using PRF0 as the fuel. The line represents where SOC from MKIM and that of TKM are the same.

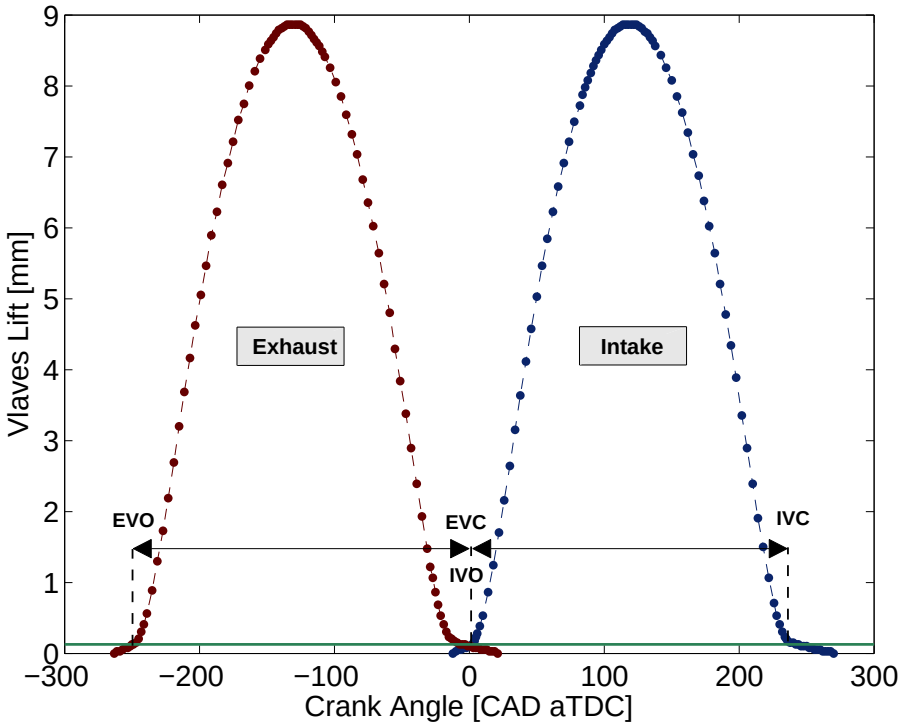

Figure 3: Measured lift profile for the valves used in this study. [The solid horizontal line shows the defined threshold ($\simeq$ 0.15 mm) for opening/closing point of valves.]

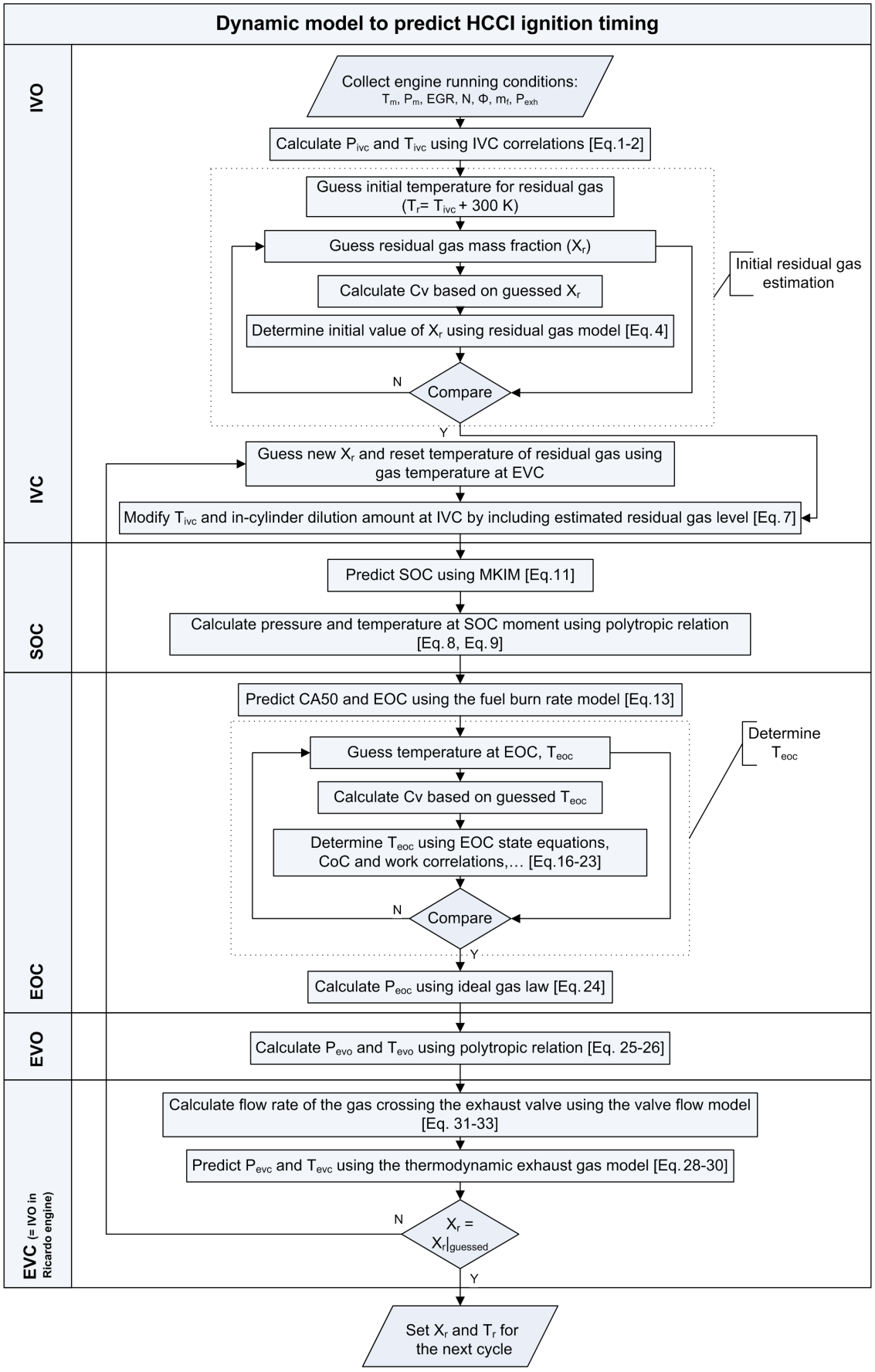

Figure 4: Schematic of the developed model.

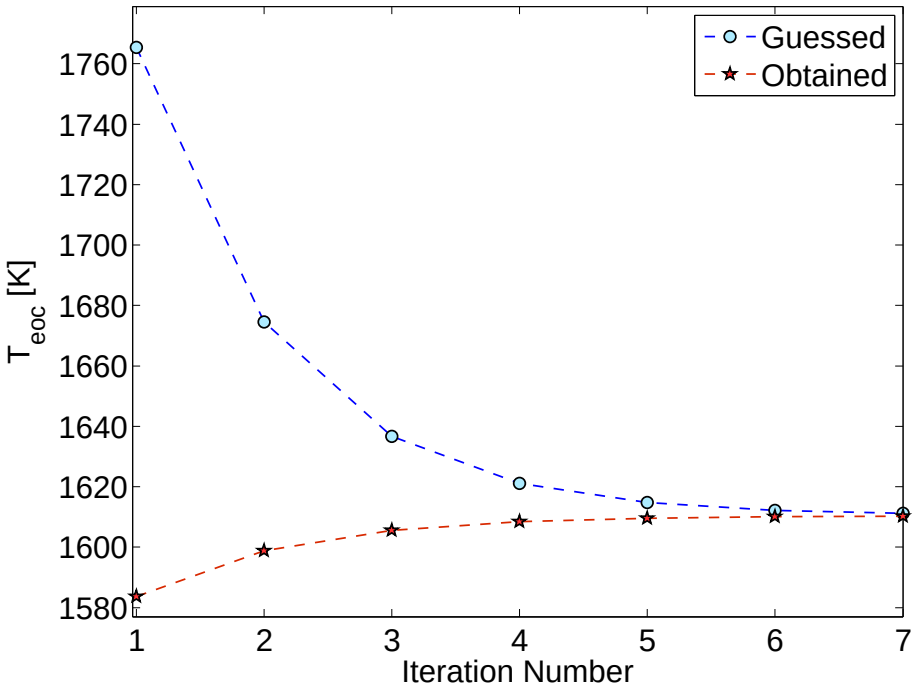

Figure 5: Simulation conversion rate for the T_{eoc} for a sample operating point. (ON = 0, N = 810 rpm, $\Phi = 0.44$, $P_m = 101$ kPa, $T_m = 102°C$)

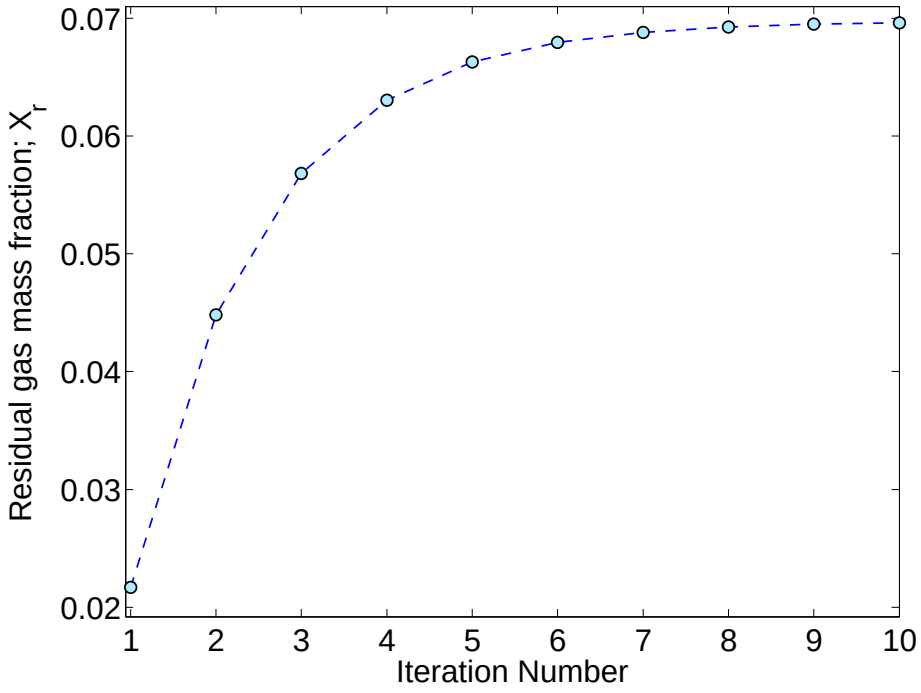

Figure 6: Conversion rate of the simulated residual gas mass fraction for a sample operating point. (ON = 0, N = 810 rpm, $\Phi = 0.44$, $P_m = 101$ kPa, $T_m = 102$°C)

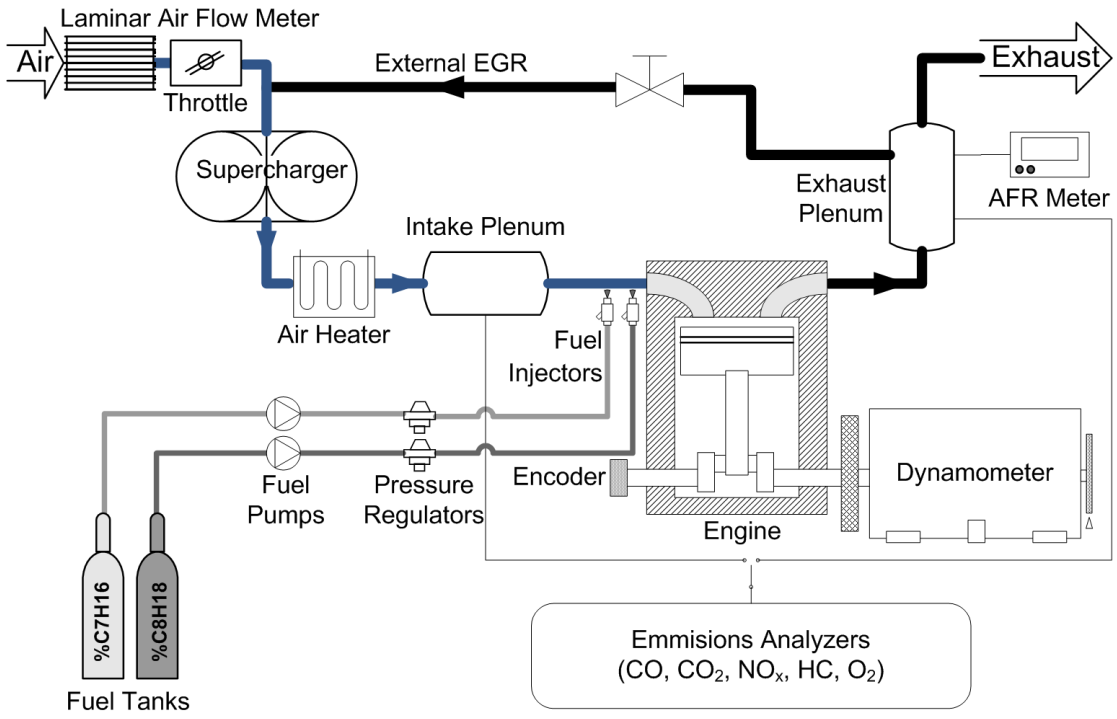

Figure 7: Ricardo single cylinder testbench schematic

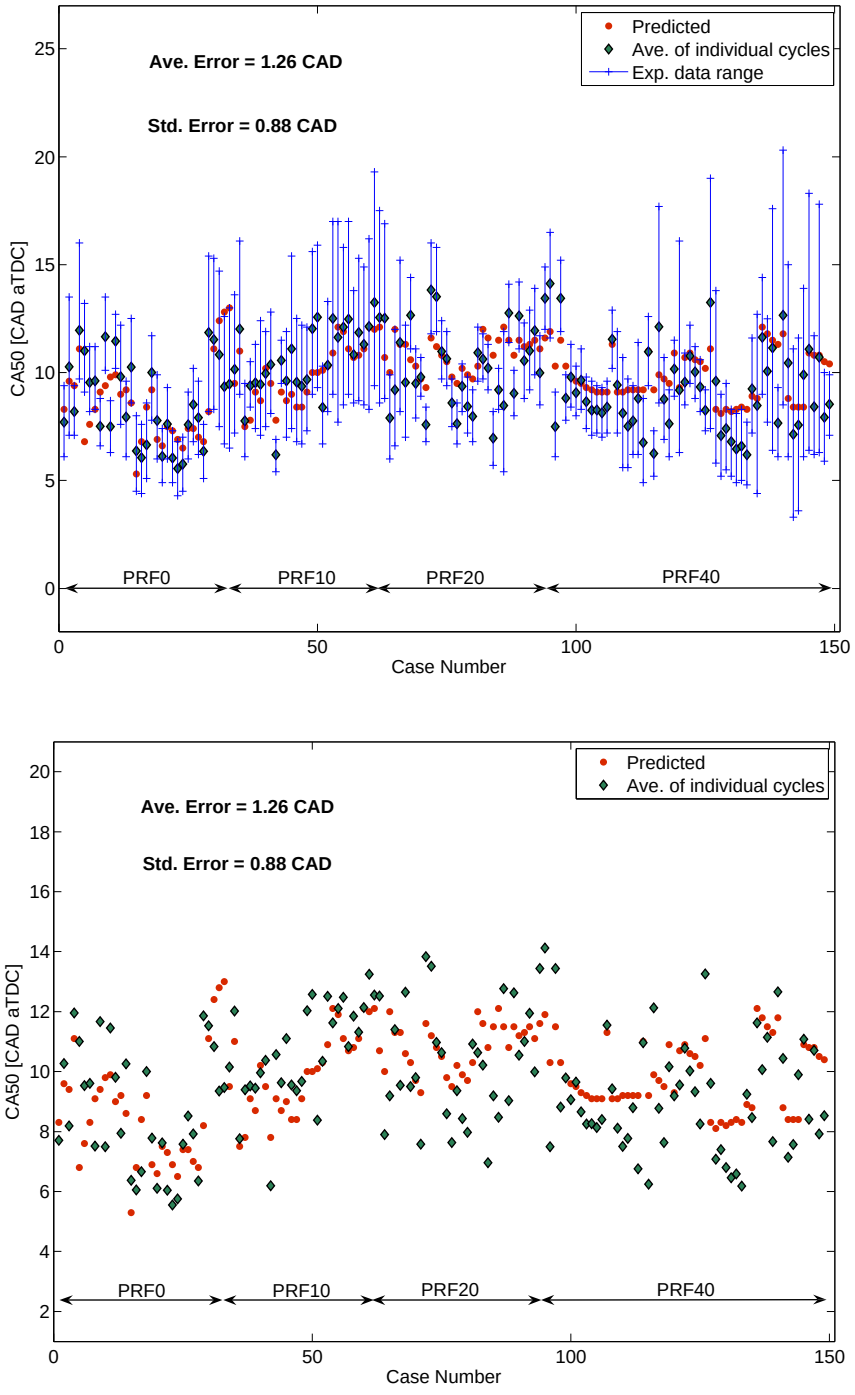

Figure 8: Comparison between predicted and experimental CA50 for four PRF blends at different steady-state engine conditions.

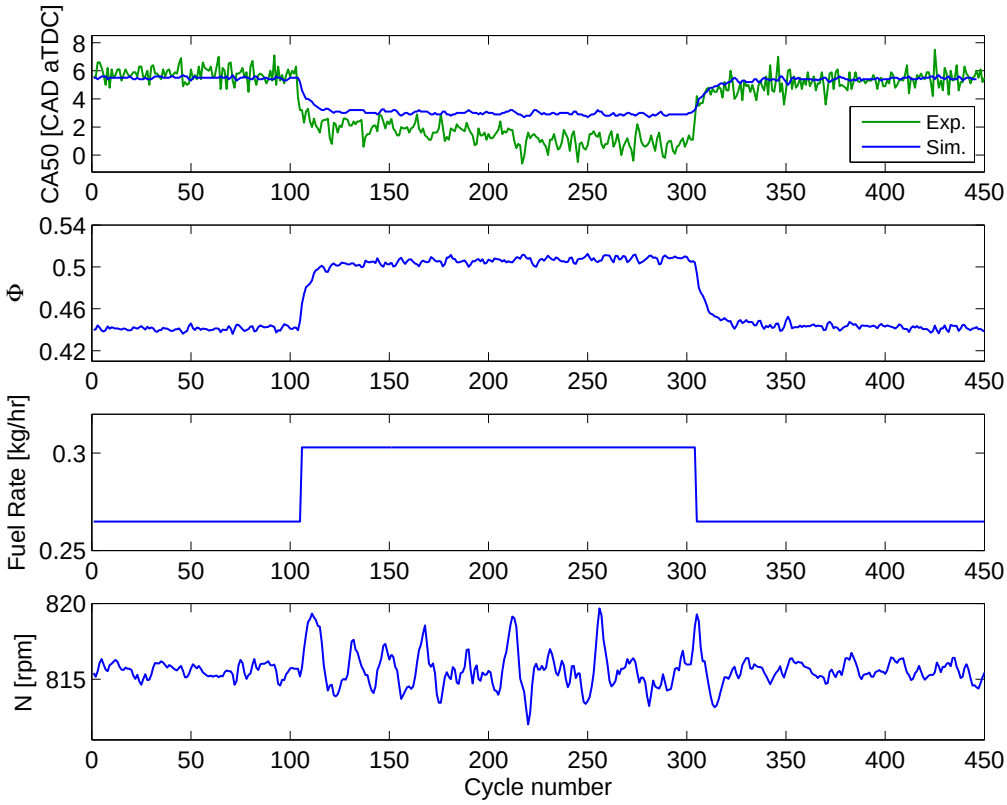

Figure 9: Equivalence ratio step: comparison between predicted and experimental cycle-by-cycle CA50. (ON = 0; P_m = 100 kPa, T_m = 67°C, EGR = 0%, P_{exh} = 97.3 kPa)

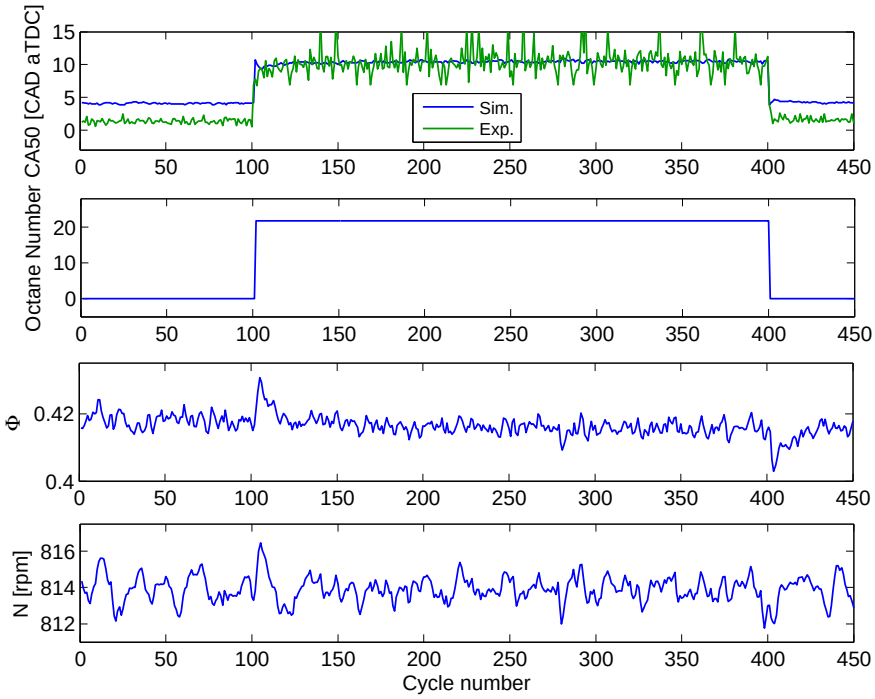

Figure 10: Octane number step: comparison between predicted and experimental cycle-by-cycle CA50. ($P_m = 110$ kPa, $T_m = 91°$C, $\Phi \cong 0.42$, EGR $= 0\%$, $P_{exh} = 99$ kPa)

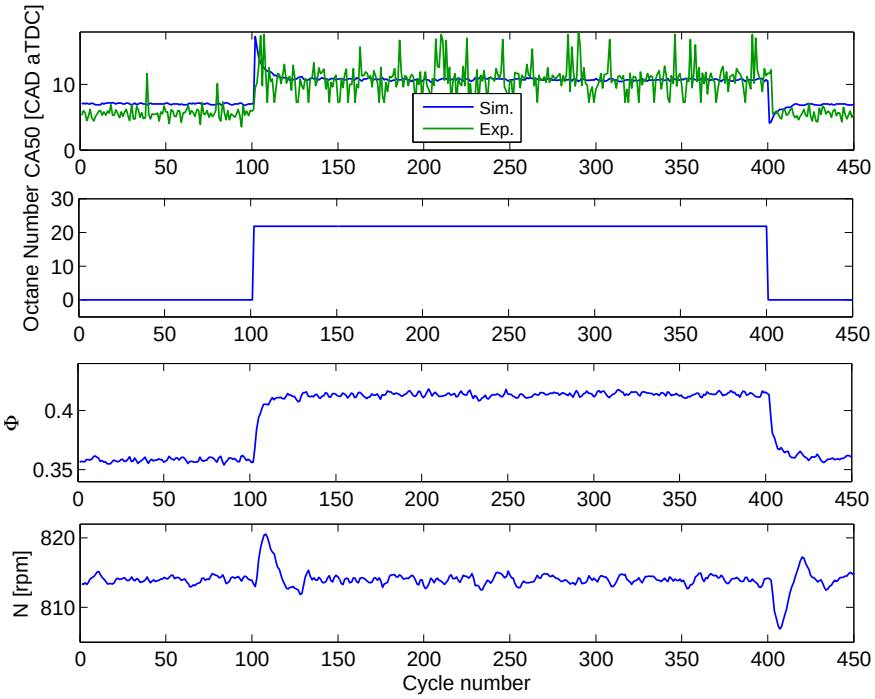

Figure 11: Octane number and equivalence ratio (Φ) step: comparison between predicted and experimental cycle-by-cycle CA50. (P_m = 110 kPa, T_m = 91°C, EGR = 0%, P_{exh} = 99 kPa)

List of Tables

List of Figures